ACS APPLIED MATERIALS & INTERFACES

Research Article

www.acsami.org

Uniform, Stable, and Efficient Planar-Heterojunction Perovskite Solar Cells by Facile Low-Pressure Chemical Vapor Deposition under Fully Open-Air Conditions

Paifeng Luo,*[,†] Zhaofan Liu,[†] Wei Xia,[†] Chenchen Yuan,[‡] Jigui Cheng,[†] and Yingwei Lu[†]

[†]Department of Materials Science and Engineering, Hefei University of Technology, Hefei, Anhui 230009, P.R. China

[‡]CAS Key Laboratory of Materials for Energy Conversion, University of Science and Technology of China, Hefei, Anhui 230026, P.R. China

Supporting Information

ABSTRACT: Recently, hybrid perovskite solar cells (PSCs) have attracted extensive attention due to their high efficiency and simple preparing process. Herein, a facile low-pressure chemical vapor deposition (LPCVD) technology is first developed to fabricate PSCs, which can effectively reduce the over-rapid intercalating reaction rate and easily overcome this blocking issue during the solution process. As a result, the prepared uniform perovskite films exhibit good crystallization, strong absorption, and long carrier diffusion length. More strikingly, $CH_3NH_3PbI_3$ absorbers by LPCVD demonstrate excellent moisture-resistant feature even under laser illumination and high-temperature conditions, which indicates that our proprietary method is very suitable for the future low-cost, nonvacuum production of the new generation photovoltaic devices. Finally, high efficiency of 12.73% is successfully achieved under fully open-air conditions. To the best of our knowledge, this is the first report of efficient PSCs with such a high humidity above 60%.

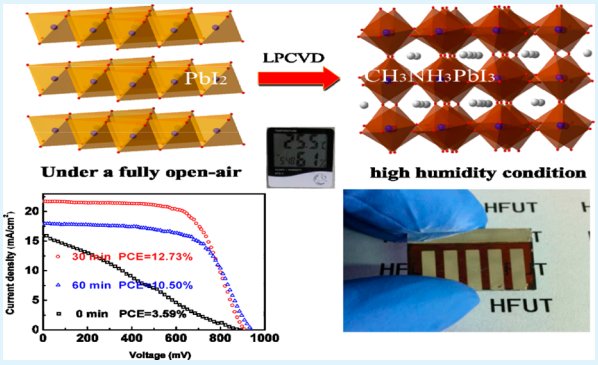

KEYWORDS: *perovskite solar cells, planar-heterojunction, low-pressure chemical vapor deposition, high-quality films, stability*

1. INTRODUCTION

Currently, the next generation hybrid organic−inorganic perovskite solar cells (PSCs) have been considered as one of the most important breakthroughs in the history of photovoltaic (PV) research due to their high efficiency, low cost, and simple preparing process.[1−3] With a common $CH_3NH_3MX_3$ (M = Pb, Sn; X = halogen) molecular formula, hybrid perovskite light absorbers afford several advantages, i.e., large absorption coefficient, suitable direct bang gap, high carrier mobility, and long-range carrier diffusion length.[4−7] In terms of excellent optical-electric properties, hybrid perovskite materials were primarily used as field-effect transistors, light-emitting diodes, and photodetectors in the past decade.[8,9] Until recently, in 2009, perovskite was first attempted as a sensitizer in dye-sensitized solar cells (DSCs) by Kojima et al.[10] Then Park and co-workers reported 6.54% efficient quantum-dot-sensitized solar cells (QDSCs) using perovskite nanocrystal sensitizer.[11] Subsequently, the solid-state mesoscopic and planar heterojunction PSCs were developed by Grätzel, Park, and Snaith and co-workers, respectively.[1,4,12] Quite recently, Yang and co-workers achieved the highly efficient PSCs with the state-of-the-art highest efficiency of 19.3%.[13] In short, the newcomer has sparked an explosion in the PV research field and shown the potential as a cost-efficient alternative to the traditional semiconductor-based solar cells.[14−16]

Although there is still some controversy about the fundamental working mechanism of PSCs, the simple planar heterojunction configuration gradually becomes the mainstream structure in recent research, which is more convenient to be applied on a rigid or flexible substrate compared with complex sensitized or nanostructured architecture.[12,17,18] But the incomplete coverage of perovskite films usually appeared in planar structure dramatically deteriorates the photovoltaic performance. Thus, it is very crucial to improve the film quality, in particular, pay attention to the uniformity, roughness, and surface coverage. Up to now, various processing approaches have been employed to prepare perovskite absorbers. Thermal evaporation method has been introduced to deposit perovskite films and can readily reach the desired high-quality level.[12,19] However, vacuum-based technology requires expensive equipment, complicated composition control, and preparing process. Solution-based spin-coating route including a one-step and two-step process is another widespread method to synthesize the perovskite absorbers.[2,20,21] But the solution method essentially encounters a blocking issue during the synthesis process, which accompanies

Received: November 6, 2014
Accepted: January 12, 2015
Published: January 12, 2015

DOI: 10.1021/am5077588
ACS Appl. Mater. Interfaces 2015, 7, 2708−2714

an over-rapid reaction rate between the inorganic framework and organic species, and always results in rough, porous, and incomplete covered films. Meanwhile, the spin-coating route is not suitable for mass production because of the uniformity issue in large area. More recently, in situ vapor-assisted solution process was developed as a fruitful way for the fabrication of perovskite absorbers.[22] Unfortunately, the fussy manipulations in a glovebox are difficult to scale up and hamper further practical applications. Therefore, development of an effective large-scale deposition technology under ambient air is of great importance for the future commercialization of PSCs.

Herein, we first present a facile LPCVD method to grow high-quality $CH_3NH_3PbI_3$ absorbers, which implies a promising route for mass production of the new generation photovoltaic devices (PVs). In fact, LPCVD is an industrial mature technology to deposit uniform thin films in large scale and has been broadly applied in the commercial production of a-Si, Si_3N_4, SiO_2, and ZnO.[23,24] Under low-pressure conditions, the dilute molecule concentration of CH_3NH_3I vapor can effectively abate the over-rapid intercalating reaction rate and obtain uniform perovskite absorbers. Therefore, the prepared films exhibit good crystallization, strong absorption, and long carrier diffusion length. Surprisingly, the compact films demonstrate a good stability even under laser illumination and high-temperature conditions. This unique characteristic shows the possibility of producing PSCs under the whole nonvacuum environment. Finally, on the basis of planar configuration, so far the highest efficiency of 12.73% is successfully achieved under a fully open-air condition with high humidity above 60%.

2. EXPERIMENTAL DETAILS

2.1. Deposition of $CH_3NH_3PbI_3$ Absorbers. First, 24 mL of methylamine (33 wt % ethanol solution) and 10 mL of hydroiodic acid (45 wt % in water) were reacted in a 100 mL beaker at 0 °C for 2 h with continuous stirring. The precipitation was then dissolved in 80 mL of ethanol and precipitated with the addition of 300 mL of diethyl ether. After the precipitation was vacuum-dried for 24 h, a white CH_3NH_3I powder was obtained. Second, PbI_2 powder was dissolved in *N*,*N*-dimethylformamide at a concentration of 462 mg/mL at 70 °C. The PbI_2 films were obtained by spin-coating twice on the c-TiO_2/fluorinated tin oxide (FTO)/glass substrate at a speed of 4000 rpm for 30 s. Finally, CH_3NH_3I powder and PbI_2 films were separately placed in the A and B zones of the tubular furnace. After pumping for 10 min, CH_3NH_3I was heated to 180 °C, while PbI_2 films were heated to 140 °C simultaneously. After reacting for 100 min, the dark brown $CH_3NH_3PbI_3$ films were taken out and washed with isopropanol, and annealed at 145 °C for different times in air.

2.2. Fabrication of PSCs. All the experiments were carried out under fully open-air conditions with humidity of about 60% at room temperature. First, 730 μL of titanium isopropoxide was added into 5 mL of ethanol, and 69 μL of HCl (2 M) was added into 5 mL of ethanol and then mixed and filtered with a 0.22 μm poly(tetrafluoroethylene) filter. The c-TiO_2 films were obtained by spin-coating on the etched FTO-coated glass sheets (15 Ω/sq) and sintering at 500 °C for 30 min, then treated in 40 mM aqueous solution of $TiCl_4$ for 30 min at 70 °C and dried at 500 °C for another 30 min. Second, $CH_3NH_3PbI_3$ absorbers were deposited on the c-TiO_2/FTO/glass substrate by LPCVD as mentioned above. Finally, hole-transport material (HTM) solution was prepared by dissolving 72.3 mg of 2,2′′,7,7′′-tetrakis(*N*,*N*-di-*p*-methoxyphenylamine)-9,9-spirobifluorene (spiro-MeOTAD) in 1 mL of chlorobenzene, to which 28.8 μL of 4-*tert*-butylpyridine and 17.5 μL of lithium bis(trifluoromethanesulfonyl)imide solution (520 mg of lithium bis(trifluoromethylsulphonyl)imide (LITSFI) in 1 mL of acetonitrile) were added, and then spin-coated at 4000 rpm for 30 s on the deposited perovskite substrate. Finally, silver electrode was deposited by thermal evaporation with a covered ultrathin stainless steel mask (active area: 0.12 cm^2).

2.3. Characterizations. The phase composition and the crystal structure were identified by the X-ray diffraction (XRD) method (D/MAX2500 V). Differential scanning calorimetric (DSC) measurement was carried out using a simultaneous thermogravimetric analyzer (NETZSCH STA449F3). The morphology and composition were separately observed by field emission scanning electron microscope (FESEM, Sirion200), SEM-energy dispersive spectroscopy (EDS), metallographic microscope (LV8000), and atomic force microscope (AFM, Dimension FastScan). The absorption spectrum was recorded by a UV−visible spectrophotometer (CARY 5000) with the wavelength range of 300∼1000 nm. Steady-state photoluminescence (PL) was analyzed using a steady-state lifetime spectrofluorometer (FlUOROLOG-3-TAU) with an exciting wavelength of 370 nm and detection at 770 nm. The transient PL spectrum was measured by a PL spectrometer (FLS920, Edinburgh Instruments Ltd.) with the same exciting and detecting wavelengths. Raman spectroscopy was measured by a Focal Laser MicroRaman Spectrometer (LABRAM-HR) with an excitation of 514.5 nm. Temperature was controlled by a Linkam THMS 600 heating and cooling stage equipped with a TMS 94 temperature controller and LNP 94 liquid nitrogen cooling system. The heating rate was 20 °C/min and the temperature was kept for 5 min at each measuring point before measurement. Photocurrent density−voltage (J−V) characteristics were recorded with a Keithley 2400 source meter under illumination of 100 mW/cm^2, AM1.5, by a solar simulator (Newport, Oriel Sol3A 94023A) in air. And J−V curves were obtained by reverse scan from 1.2 to −0.1 V and/or forward detection from −0.1 to 1.2 V. The step voltage was fixed at 10 mV and the active area of single cells is 0.12 cm^2.

3. RESULTS AND DISCUSSION

In Figure 1, the home-built LPCVD equipment is essentially derived from the traditional double-zone CVD tubular furnace,

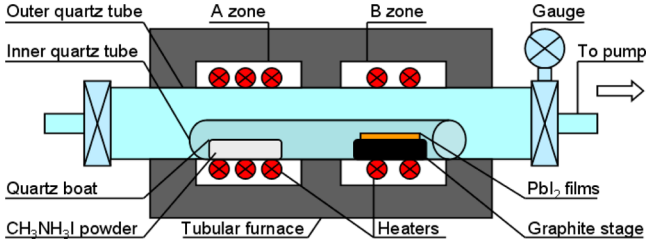

Figure 1. Schematic diagram of home-built LPCVD equipment.

which is so simple and easy to be scale up for mass production. The synthesized CH_3NH_3I white powder is loaded in the quartz boat as vapor source and also characterized by XRD and DSC, as shown in Figures S1, S2, and S3 of the Supporting Information. To avoid its phase transition temperature, CH_3NH_3I powder is heated to 180 °C to supply enough vapor pressure. As mentioned above, the whole reaction

DOI: 10.1021/am5077588
ACS Appl. Mater. Interfaces 2015, 7, 2708−2714

process in the solution route is very fast and usually accomplished in 1 min. But the over-rapid reaction rate will enhance the surface roughness and lead to pinhole formation. In contrast, the reaction rate of LPCVD is dominated by the slow gas−solid (G−S) reaction. Under low-pressure conditions, the long molecular free path of CH_3NH_3I vapor can eventually eliminate the gas concentration gradient, and slowly react with PbI_2 films through the layer-by-layer growth. So after 15−20 min, the color of samples just starts to change, and then it needs another 45−100 min to finish the slow G−S reaction. The photograph in Figure S4 of the Supporting Information records the whole detailed reaction process. From the pictures we can see that there is no obvious color difference among the same batch pieces. Therefore, our facile LPCVD technology demonstrates good uniformity and reproducibility, which is expected to grow high-quality perovskite films.

The crystal structures and photographs of PbI_2 films and $CH_3NH_3PbI_3$ absorbers are shown in Figure 2a−d. Generally,

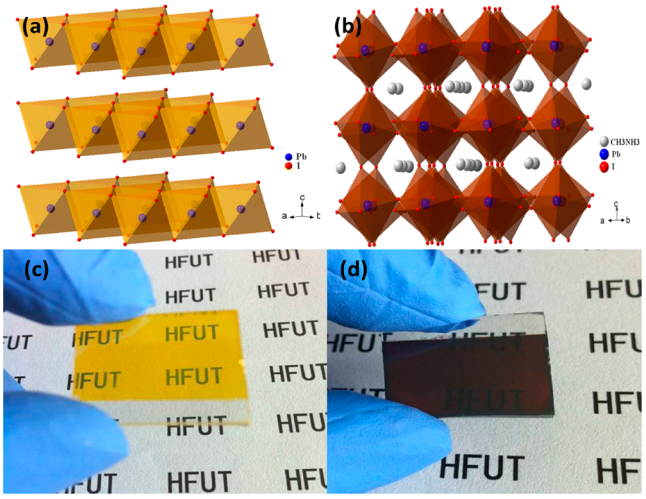

Figure 2. Crystal structures of (a) hexagonal PbI_2 and (b) perovskite $CH_3NH_3PbI_3$, and their photographs of (c) PbI_2 films and (d) $CH_3NH_3PbI_3$ absorbers.

PbI_2 has a hexagonal structure with space group $P\bar{3}m1(164)$, while $CH_3NH_3PbI_3$ pertains to the orthorhombic perovskite structure with space group *Pbnm*(62). On the basis of the reported data, the crystal structures of PbI_2 and $CH_3NH_3PbI_3$ viewed from the (110) plane are drawn in parts (a) and (b), separately, of Figure 2.[25,26] In general, the intercalating reaction always occurs through the diffusion of CH_3NH_3I molecule to the $PbI_2/CH_3NH_3PbI_3$ interface. The huge distance between layered PbI_2 films can supply enough space to accommodate CH_3NH_3I molecule. Thus, the reaction of the fabrication of $CH_3NH_3PbI_3$ perovskite absorbers belongs to a typical intercalating reaction. Meanwhile, to further analyze the crystal structure, XRD of PbI_2 films and $CH_3NH_3PbI_3$ absorbers is detected and shown in Figure 3. From the XRD pattern of PbI_2 films, deducting the diffractions of TiO_2/FTO/glass substrate, the observed main peaks (001) at 12.62°, (002) at 25.4°, (003) at 38.54°, and (004) at 52.30° are highly compatible with the layered hexagonal structure and have a preferential orientation along the *c*-axis. While $CH_3NH_3PbI_3$ gives peaks at 14.07°, 28.36°, 31.82°, and 43.14°, assigned as the (110), (220), (310), and (330) planes, and shows an orthorhombic crystal structure with preferred (110) orientation. So during the intercalating

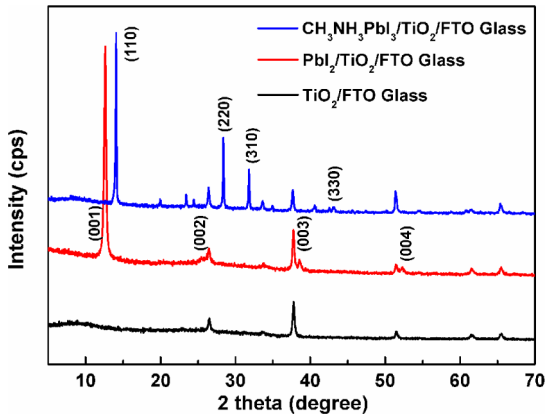

Figure 3. XRD patterns of TiO_2/FTO/glass (black line), PbI_2/TiO_2/FTO/glass (red line), and $CH_3NH_3PbI_3/TiO_2$/FTO/glass (blue line).

reaction process, CH_3NH_3I vapor molecule slowly diffuses into the layered structure along the van der Waals gap, and eventually presents homogeneous perovskite films.[27] After the reaction finished, all the identical peaks of PbI_2 disappeared and many new diffractions of $CH_3NH_3PbI_3$ are observed, which means the conversion from hexagonal PbI_2 into perovskite structure was completed.

As mentioned above, the morphology and composition of light absorbers are the key factors for achieving high-efficient solar cells, especially for planar heterojunction architecture. So the smooth, compact, and nonporous perovskite films must be achieved to avoid the shunting current arising from direct contact between the hole-transport material (HTM) and TiO_2. However, current solution-based route always produces oversized grains and uncovered pinholes.[2,20] In contrast, perovskite films by the LPCVD method demonstrates very good morphology, which has been sequentially verified by SEM, AFM, and metallurgical microscope, as shown in Figures 4 and 5. From the low- and high-magnification SEM in Figure 4, we can clearly observe that the super uniform, homogeneous, and well-dined $CH_3NH_3PbI_3$ layers are fully covered on the TiO_2/FTO/glass substrate. Usually, most of the reported so-called high-quality works still have some obvious small cracks or

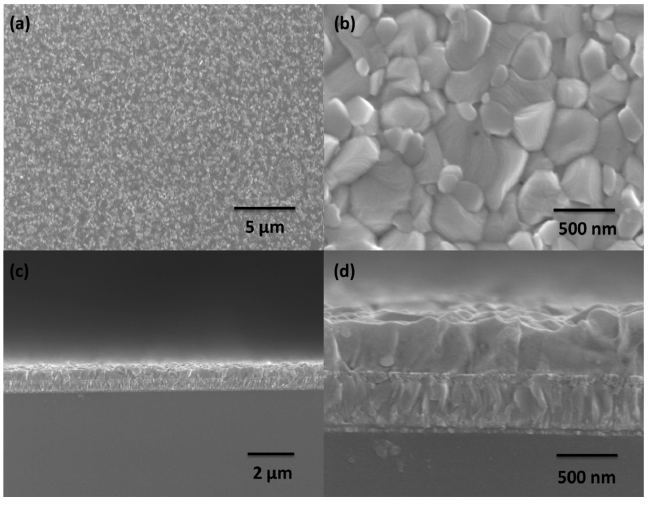

Figure 4. (a) Low- and (b) high-magnification planar SEM. (c) Low- and (d) high-magnification cross-sectional SEM of $CH_3NH_3PbI_3$ absorbers.

DOI: 10.1021/am5077588
ACS Appl. Mater. Interfaces 2015, 7, 2708−2714

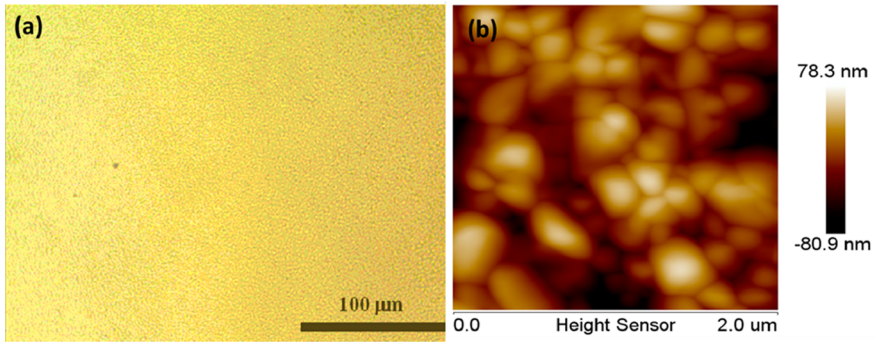

Figure 5. (a) Metallurgical micrograph and (b) 2D AFM height image (2 × 2 μm) of $CH_3NH_3PbI_3$ absorbers.

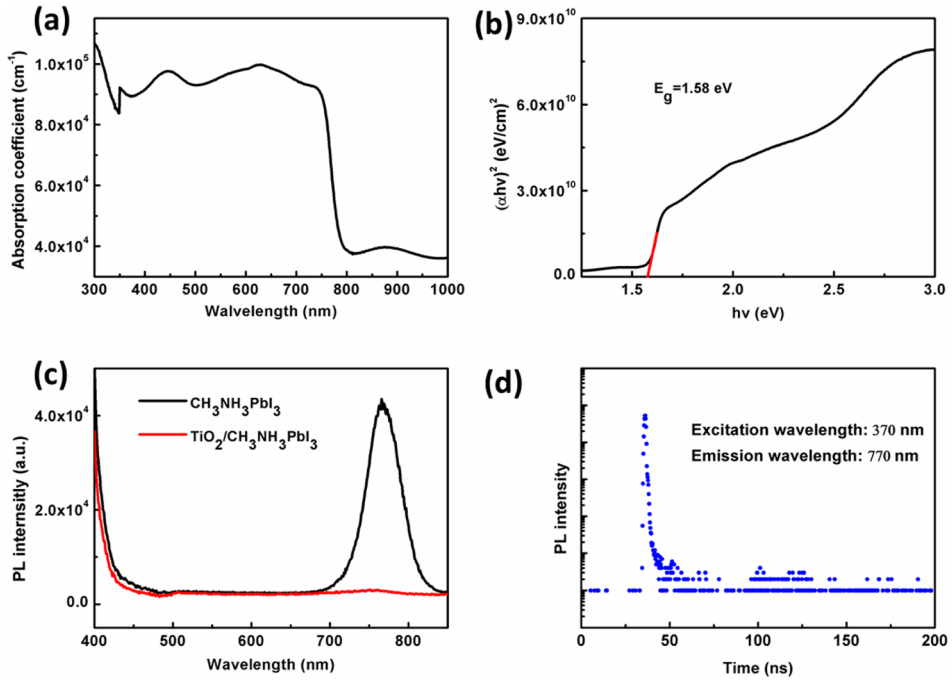

Figure 6. (a) Wavelength dependence of the absorption coefficient and (b) $(\alpha h\nu)^2$ vs $h\nu$ of optical absorption spectra and (c) steady-state and (d) transient photoluminescence of $CH_3NH_3PbI_3$ films.

pinholes in their $CH_3NH_3PbI_3$ absorbers. Surprisingly, our films are extremely dense and compact, with super uniformity even in a large scale as shown in the metallurgical micrograph of Figure 5a. At the same time, the grain size of $CH_3NH_3PbI_3$ films is also very uniform, and almost all of them attain up to 500 nm, which indicates a high level of crystallization. From the two-dimensional (2D) AFM height image in Figure 5b, the calculated roughness of the homogeneous films is only 19.6 nm. Meanwhile, the bearing depth over 2 × 2 μm three-dimensional AFM graph is also just 78 nm, as shown in Figure S5 of the Supporting Information. In addition, according to the EDS result shown in Figure S6, the Pb/I ratio is very close to the desired stoichiometry and the prepared $CH_3NH_3PbI_3$ absorbers have good composition. In brief, our perovskite films by LPCVD method demonstrate top-level quality and are comparable to that prepared by vacuum thermal evaporation technology.

The optical properties of $CH_3NH_3PbI_3$ films are characterized by UV−vis spectrophotometer and steady-state and transient photoluminescence (PL), as shown in Figure 6a−d. Generally, perovskite quantum dots or films with poor quality have a limited absorption coefficient of 1−2 × 10^4 cm^{-1} and a narrow absorption region.[7,11] As comparison, here our films show a broad strong absorption covering the entire visible range, and have an average value of 9−10 × 10^4 cm^{-1} as shown in Figure 6a,b, which must result from the compact and uniform high film quality. The band gap (E_g) of 1.58 eV is also obtained from the equation: $\alpha h\nu = A(h\nu - E_g)^{1/2}$, where $h\nu$ is the photon energy and A is an arbitrary constant. In Figure 6c, the PL spectrum of $CH_3NH_3PbI_3$ films is right at the band edge only with little Stokes shift and shows a strong and symmetric band at 720−820 nm with apeak of 766 nm, which implies that the photoinduced carriers are accumulating at the band edge and lighting through direct recombination.[6,21] To determine the compatibility of perovskite absorbers with electron acceptors in the PVs, the PL quenching of perovskite emission in $TiO_2/CH_3NH_3PbI_3$ bilayers structure is also detected, as represented by the red line in Figure 6c. The emission band of $TiO_2/CH_3NH_3PbI_3$ bilayers is very flat and straight, only with a little bulge at 760 nm, which illustrates the good compatibility of charge transfer from $CH_3NH_3PbI_3$ to TiO_2. Moreover, from transient PL spectra as shown in Figure 6d, the effective lifetime of carriers with 34 ns can be deduced (the time taken for the PL to fall to 1/e of its initial intensity), which is detected at the

DOI: 10.1021/am5077588
ACS Appl. Mater. Interfaces 2015, 7, 2708−2714

peak emission of 770 nm by the time-correlated single-photon counting technique. So a long electron diffusion length of 240 nm is received, which is remarkably longer than the reported distance of 100 nm in $CH_3NH_3PbI_3$ films.[6,7,21] Note that the films without encapsulation are stored in a desiccator all the time before PL characterization. In a word, our films exhibit a large broad absorption, strong PL emission, good charge transfer compatibility, and long carrier diffusion length, which should be the ideal candidate for the light harvester.

The stability of perovskite materials has been regarded as one of the most challenging problems for the future commercialized applications, but so far only very few studies have focused on this issue. Herein, to the best of our knowledge, variable-temperature Raman spectrum is for the first time to be applied to examine the structural changes of perovskite films. As shown in Figure 7, $CH_3NH_3PbI_3$ films show strong peaks at 96, 112, 167, and 217 cm^{-1} at room temperature. The band at 96 cm^{-1} is assigned to the bending and stretching of Pb−I bonds, which is the diagnostic mode of the inorganic cages. The broad unstructured 200−400 cm^{-1} feature is assigned to the torsional mode of methylammonium cations.[28] As the temperature is raised from 25 to 180 °C in air, surprisingly, the crystal structure of $CH_3NH_3PbI_3$ films is very stable even under laser irradiation with high temperature above 70 °C.

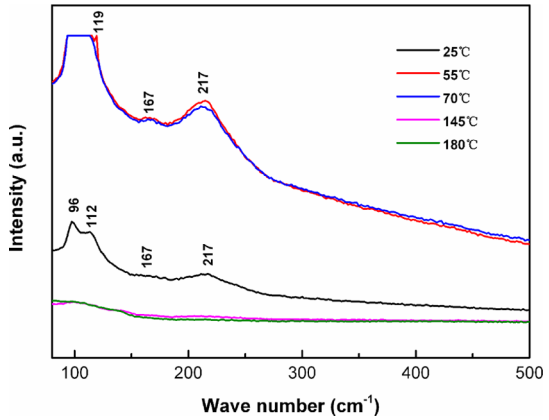

Figure 7. Variable-temperature Raman spectra of $CH_3NH_3PbI_3$ films.

Until heated up to 145 °C for 5 min, the perovskite structure starts to be destroyed. As the temperature rose to 180 °C, all the main peaks disappeared. So under laser illumination, our films are relatively stable but cannot endure high temperature above 180 °C. On the other hand, since the vibration peaks of perovskite in Raman spectra are quite similar to that of PbI_2 probably due to the similarity in their crystal structures, the structural changes of $CH_3NH_3PbI_3$ films at different annealing times are further scrutinized by XRD.[29] In Figure 8, after the films are heated at 145 °C in air with humidity of 61% for 30 min, weak signals of PbI_2 at 12.62° and 38.54° begin to appear. With a prolonged heating time, the diffractions of PbI_2 are gradually enhanced, while the main peaks of $CH_3NH_3PbI_3$ still can be observed even after heating at 145 °C for 120 min. Figure S7 in the Supporting Information shows (a−d) the appearance of $CH_3NH_3PbI_3$ films at different annealing times and (e) a photograph of the annealing process. From the photographs taken from outside the quartz tube, there are no apparent color changes among the samples. Generally, the annealing temperature in the solution route is processed at 70 °C in a glovebox or dry air conditions. $CH_3NH_3PbI_3$ films with poor quality will decompose quickly in ambient open air, especially under high humidity conditions. Therefore, our films prepared by LPCVD have a better moisture-resistant ability and are suitable for the nonvacuum process of PSCs.

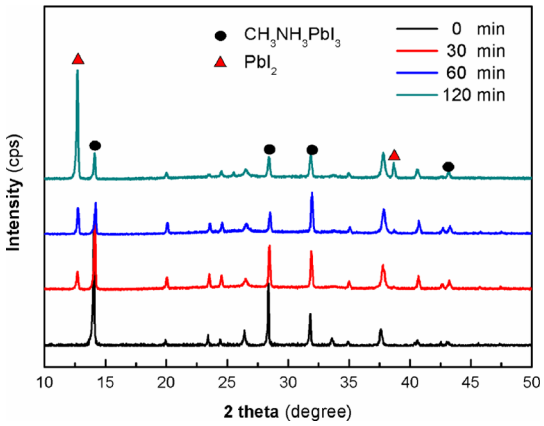

Figure 8. XRD patterns of $CH_3NH_3PbI_3/TiO_2/FTO/glass$ at different annealing time.

In the end, the PSCs are assembled by sequentially spin-coating the HTM layer (spiro-MeOTAD) and evaporating Ag electrode. The effect of PbI_2 on the device performance is also investigated in this part. As comparison, perovskite films annealed for 0, 30, and 60 min are used to fabricate solar cells and their performance data are shown in Table 1. The J−V curves of the best PSCs are obtained in Figure 9a (reverse scan). PSCs without annealing give limited efficiency of 3.59%, which are presumably due to a large amount of charge traps and the high carrier recombination consisted in the perovskite absorbers. In contrast, all the annealed PSCs show higher efficiencies above 9% and exhibit good repeatability. Most of our PVs give open voltage (V_{oc}) of 890−960 mV, short current density (J_{sc}) of 17.5−21.8 mA/cm^2, and filling factor (FF) of 0.50−0.66. The best device, as shown in Figure 9b, is obtained from annealing for 30 min, which provides a high PCE of 12.73% with V_{oc} of 910 mV, J_{sc} of 21.7 mA/cm^2, and FF of 0.645. Importantly, almost all the reported efficient PSCs are fabricated in a glovebox or dry air with low humidity below 30%. Thus, this is the highest efficiency so far, all made from fully open-air conditions with high humidity above 60%. The enhanced efficiency benefited from the high film quality and the presence of PbI_2. Recent works have explained the passivation effect of PbI_2 in PSCs, which can effectively reduce the carrier recombination in the perovskite absorbers.[30,31] At the same time, the reverse and forward scan J−V characteristics are also detected to investigate the hysteresis effect. Figures S8 and S9 of the Supporting Information show the J−V curves of the best PSCs annealing for 30 min, and the PSCs annealing for (a) 0 and (b) 60 min with reverse and forward scan mode, respectively. Here, we can see that PSCs without annealing have serious hysteresis phenomenon, while the hysteresis effect in the annealed PSCs is significantly relieved. The 11.1% lower efficiency of the best PSCs with forward scan mode mainly comes from the lower FF. Moreover, PSCs of annealing for 60 min still show the efficiency of 10.5% with V_{oc}, J_{sc}, and FF of 940 mV, 18 mA/cm^2, and 0.62, respectively, which again strongly verifies the stability and high quality of our perovskite materials.

DOI: 10.1021/am5077588
ACS Appl. Mater. Interfaces 2015, 7, 2708−2714

Table 1. Performance Data for PSCs Annealed at Different Times[a]

annealed time	V_{oc} (V)	J_{sc} (mA/cm^2)	FF PCE (%)	[Best-PCE]
0 min	0.896 ± 0.009	15.47 ± 0.88	25.12 ± 0.82	3.47 [3.59]
30 min	0.925 ± 0.025	20.92 ± 0.82	60.92 ± 4.75	11.81 [12.73]
60 min	0.925 ± 0.037	18.07 ± 0.53	56.58 ± 6.09	9.49 [10.50]

[a]Each value represents the average from five cells.

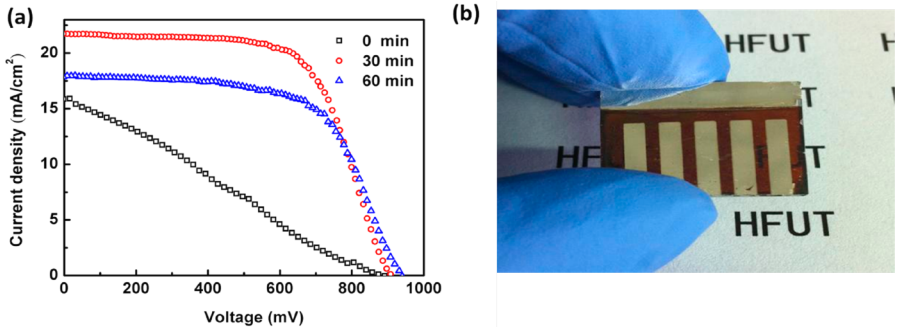

Figure 9. (a) J−V curves of PSCs with different annealing times and (b) photograph of the best PSCs.

4. CONCLUSIONS

Without need of the fussy glovebox or expensive vacuum equipment, a facile LPCVD technology is first developed to fabricate PSCs. The prepared $CH_3NH_3PbI_3$ absorbers demonstrate top-level quality and exhibit excellent optical-electric properties. More importantly, our films have a unique moisture-resistant feature and can be used in the nonvacuum process. At last, so far the highest efficiency of 12.73% is successfully achieved under fully open-air conditions with high humidity above 60%. Therefore, our work not only can realize the simple preparation of PSCs in more common laboratories but also makes a remarkable leap forward for future commercial applications.

■ ASSOCIATED CONTENT

Supporting Information

Figures S1−S9. This material is available free of charge via the Internet at http://pubs.acs.org.

■ AUTHOR INFORMATION

Corresponding Author

*E-mail: lpfeng@hfut.edu.cn.

Author Contributions

The manuscript was written and approved by all authors.

Notes

The authors declare no competing financial interest.

■ ACKNOWLEDGMENTS

This work was financially supported by the National Natural Science Foundation of China (51302058) and the Opening Project of CAS Key Laboratory of Materials for Energy Conversion at University of Science and Technology of China (USTC).

■ REFERENCES

(1) Lee, M. M.; Teuscher, J.; Miyasaka, T.; Murakami, T. N.; Snaith, H. J. Efficient Hybrid Solar Cells Based on Meso-superstructured Organometal Halide Perovskites. *Science* **2012**, *338*, 643−647.

(2) Burschka, J.; Pellet, N.; Moon, S. J.; Baker, R. H.; Gao, P.; Nazeeruddin, M. K.; Gratzel, M. Sequential Deposition as a Route to High-performance Perovskite-Sensitized Solar Cells. *Nature* **2013**, *499*, 316−319.

(3) Zhang, F.; Yang, X.; Wang, H.; Cheng, M.; Zhao, J.; Sun, L. Structure Engineering of Hole-Conductor Free Perovskite-Based Solar Cells with Low-Temperature-Processed Commercial Carbon Paste As Cathode. *ACS Appl. Mater. Interfaces* **2014**, *6*, 16140−16146.

(4) Kim, H. S.; Lee, C. R.; Im, J. H.; Lee, K. B.; Moehl, T.; Marchioro, A.; Moon, S. J.; Baker, R. H.; Yum, J. H.; Moser, J. E.; Grätzel, M.; Park, N. G. Lead Iodide Perovskite Sensitized All-Solid-State Submicron Thin Film Mesoscopic Solar Cell with Efficiency Exceeding 9%. *Sci. Rep.* **2012**, *2*, 591−597.

(5) Heo, J. H.; Im, S. H.; Noh, J. H.; Mandal, T. N.; Lim, C. S.; Chang, J. A.; Lee, Y. H.; Kim, H.; Sarkar, A.; Nazeeruddin, M. K.; Grätzel, M.; Seok, S. I. Efficient Inorganic-Organic Hybrid Heterojunction Solar Cells Containing Perovskite Compound and Polymeric Hole Conductors. *Nat. Photonics* **2013**, *7*, 486−491.

(6) Stranks, S. D.; Eperon, G. E.; Grancini, G.; Menelaou, C.; Alcocer, M. J. P.; Leijtens, T.; Herz, L. M.; Petrozza, A.; Snaith, H. J. Electron-Hole Diffusion Lengths Exceeding 1 Micrometer in an Organometal Trihalide Perovskite Absorber. *Science* **2013**, *342*, 341−344.

(7) Xing, G.; Mathews, N.; Sun, S.; Lim, S. S.; Lam, Y. M.; Grätzel, M.; Mhaisalkar, S.; Sum, T. C. Long-range Balanced Electron- and Hole-transport Lengths in Organic-Inorganic $CH_3NH_3PbI_3$. *Science* **2013**, *342*, 344−347.

(8) Mitzi, D. B. Templating and Structural Engineering in Organic-Inorganic Perovskites. *J. Chem. Soc., Dalton Trans.* **2001**, *1*, 1−12.

(9) Stoumpos, C. C.; Malliakas, C. D.; Kanatzidis, M. G. Semiconducting Tin and Lead Iodide Perovskites with Organic Cations: Phase Transitions, High Mobilities, and Near-Infrared Photoluminescent Properties. *Inorg. Chem.* **2013**, *52*, 9019−9038.

(10) Kojima, A.; Teshima, K.; Shirai, Y.; Miyasaka, T. Organometal Halide Perovskites as Visible-Light Sensitizers for Photovoltaic Cells. *J. Am. Chem. Soc.* **2009**, *131*, 6050−6951.

(11) Im, J. H.; Lee, C. R.; Lee, J. W.; Park, S. W.; Park, N. G. 6.5% Efficient Perovskite Quantum-Dot-Sensitized Solar Cell. *Nanoscale* **2011**, *3*, 4088−4093.

(12) Liu, M.; Johnston, M. B.; Snaith, H. J. Efficient Planar Heterojunction Perovskite Solar Cells by Vapour Deposition. *Nature* **2013**, *501*, 395−398.

(13) Zhou, H.; Chen, Q.; Li, G.; Luo, S.; Song, T.; Duan, H. S.; Hong, Z.; You, J.; Liu, Y.; Yang, Y. Interface Engineering of Highly Efficient Perovskite Solar Cells. *Science* **2014**, *345*, 542−546.

DOI: 10.1021/am5077588
ACS Appl. Mater. Interfaces 2015, 7, 2708−2714

(14) Jeon, N. J.; Noh, J. H.; Kim, Y. C.; Yang, W. S.; Ryu, S.; Seok, S. Solvent Engineering for High-Performance Inorganic-Organic Hybrid Perovskite Solar Cells. *Nat. Mater.* **2014**, *13*, 897−903.
(15) Christians, J. A.; Fung, R. C. M.; Kamat, P. V. An Inorganic Hole Conductor for Organo-Lead Halide Perovskite Solar Cells. Improved Hole Conductivity with Copper Iodide. *J. Am. Chem. Soc.* **2014**, *136*, 758−764.
(16) Carmona, C. R.; Malinkiewicz, O.; Betancur, R.; Longo, G.; Momblona, C.; Jaramillo, F.; Camachob, L.; Bolink, H. J. High Efficiency Single-Junction Semitransparent Perovskite Solar Cells. *Energy Environ. Sci.* **2014**, *7*, 2968−2973.
(17) Shi, J.; Dong, J.; Lv, S.; Xu, Y.; Zhu, L.; Xiao, J.; Xu, X.; Wu, H.; Li, D.; Luo, Y.; Meng, Q. Hole-Conductor-Free Perovskite Organic Lead Iodide Heterojunction Thin-Film Solar Cells: High Efficiency and Junction Property. *Appl. Phys. Lett.* **2014**, *104*, 063901-5.
(18) Yamada, Y.; Nakamura, T.; Endo, M.; Wakamiya, A.; Kanemitsu, Y. Photocarrier Recombination Dynamics in Perovskite $CH_3NH_3PbI_3$ for Solar Cell Applications. *J. Am. Chem. Soc.* **2014**, *136*, 11610−11613.
(19) Chen, C. W.; Kang, H. W.; Hsiao, S. Y.; Yang, P. F.; Chiang, K. M.; Lin, H. W. Efficient and Uniform Planar-Type Perovskite Solar Cells by Simple Sequential Vacuum Deposition. *Adv. Mater.* **2014**, *246*, 6647−6652.
(20) Xiao, M.; Huang, F.; Huang, W.; Dkhissi, Y.; Zhu, Y.; Etheridge, J.; Weale, A. G.; Bach, U.; Cheng, Y. B.; Spiccia, L. A Fast Deposition-Crystallization Procedure for Highly Efficient Lead Iodide Perovskite Thin-Film Solar Cells. *Angew. Chem.* **2014**, *126*, 10056−10061.
(21) Shi, J.; Luo, Y.; Wei, H.; Luo, J.; Dong, J.; Lv, S.; Xiao, J.; Xu, Y.; Zhu, L.; Xu, X.; Wu, H.; Li, D.; Meng, Q. Modified Two-Step Deposition Method for High-Efficiency $TiO_2/CH_3NH_3PbI_3$ Heterojunction Solar Cells. *ACS Appl. Mater. Interfaces* **2014**, *6*, 9711−9718.
(22) Chen, Q.; Zhou, H.; Hong, Z.; Luo, S.; Duan, H. S.; Wang, H. H.; Liu, Y.; Li, G.; Yang, Y. Planar Heterojunction Perovskite Solar Cells via Vapor-Assisted Solution Process. *J. Am. Chem. Soc.* **2014**, *136*, 622−625.
(23) Jensen, K. F.; Graves, D. B. Modeling and Analysis of Low Pressure CVD Reactors. *J. Electrochem. Soc.* **1983**, *130*, 1950−1957.
(24) Fay, S.; Steinhauser, J.; Nicolay, S.; Ballif, C. Polycrystalline ZnO: B Grown by LPCVD as TCO for Thin Film Silicon Solar Cells. *Thin Solid Films* **2010**, *518*, 2961−2966.
(25) Wyckoff, G. R. W. *New York Note: Cadmium Iodide Structure*. Interscience Publishers: New York, 1963.
(26) Sasaki, S.; Prewitt, C. T.; Bass, J. D.; Schulze, W. A. Orthorhombic Perovskite $CaTiO_3$ and $CdTiO_3$: Structure and Space Group. *Acta Crystallogr., Sect. C: Cryst. Struct. Commun.* **1987**, *43*, 1668−1674.
(27) Liang, K.; Mitzi, D. B.; Prikas, M. T. Synthesis and Characterization of Organic-Inorganic Perovskite Thin Films Prepared Using a Versatile Two-Step Dipping Technique. *Chem. Mater.* **1998**, *10*, 403−411.
(28) Quarti, C.; Grancini, G.; Mosconi, E.; Bruno, P.; Ball, J. M.; Lee, M. M.; Snaith, H. J.; Petrozza, A.; Angelis, F. D. The Raman Spectrum of the $CH_3NH_3PbI_3$ Hybrid Perovskite: Interplay of Theory and Experiment. *J. Phys. Chem. Lett.* **2014**, *5*, 279−284.
(29) Ha, S.; Liu, X.; Zhang, Q.; Giovanni, D.; Sum, T. C.; Xiong, Q. Synthesis of Organic-Inorganic Lead Halide Perovskite Nanoplatelets: Towards High-Performance Perovskite Solar Cells and Optoelectronic Devices. *Adv. Opt. Mater.* **2014**, *2*, 838−844.
(30) Wang, L.; McCleese, C.; Kovalsky, A.; Zhao, Y.; Burda, C. Femtosecond Time-Resolved Transient Absorption Spectroscopy of $CH_3NH_3PbI_3$ Perovskite Films: Evidence for Passivation Effect of PbI_2. *J. Am. Chem. Soc.* **2014**, *136*, 12205−12208.
(31) Chen, Q.; Zhou, H.; Song, T. B.; Luo, S.; Hong, Z.; Duan, H. S.; Dou, L.; Liu, Y.; Yang, Y. Controllable Self-Induced Passivation of Hybrid Lead Iodide Perovskite toward High Performance Solar Cells. *Nano Lett.* **2014**, *14*, 4158−4163.

DOI: 10.1021/am5077588
ACS Appl. Mater. Interfaces 2015, 7, 2708−2714